

08,14

***In situ* diagnostics of the deformation-induced surface evolution of polycrystalline copper during plastic flow**

© I.S. Yasnikov, E.A. Agletdinov, A.V. Danyuk

Togliatti State University,
Togliatti, Russia

E-mail: yasnikov@phystech.edu

Received March 9, 2024

Revised April 19, 2024

Accepted April 22, 2024

The paper presents an experimental implementation of a technique for diagnosing the surface of a polycrystalline copper sample during its plastic flow using an optical profilometer based on the principle of scanning white light interferometry (SWLI) and fractal dimension (self-similarity structure) analysis. A distinctive feature of the presented method is the deformation of the sample using a compact tensile testing machine with a mechanism for opposite stroke traverses, which reduces any displacement of test area of the sample in observation field of scanning white light interferometer during testing. This was provide to mine data of the same surface area during deformation and avoid a number of experimental artifacts. From the experimental data, the values of the fractal dimension were obtained using various modern computational methods, and possible correlations between the experimental data obtained in this work and the data of other researchers were indicated.

Keywords: plastic flow, fractal dimension, self-similar structures, polycrystalline copper, dislocation, fractals, scanning white light interferometry, opposite movement of traverses.

DOI: 10.61011/PSS.2024.05.58506.48

1. Introduction

A deformed solid body is a sophisticated complex system where all variety of processes may take place as addressed by the current material physics and nonlinear dynamics [1–3]. In particular, for deformation of metallic materials, main structural changes in their state are described by defect assembly evolution that is represented by a wide class of kinetic equations [4–8] that may be derived, in particular, from thermodynamic considerations [9]. However, plastic deformation of metallic materials is a spatially inhomogeneous and time-intermittent process due to the discrete nature of motion of plastic deformation carriers — dislocations [10–12]. It is the discrete nature of dislocation processes that is the cause of local strain and stress fluctuations resulting from dislocation density fluctuations. Finally, the dislocation density fluctuations, which increase in amplitude during plastic deformation, become unstable [13,14] and this microscopic effect results in macroscopic effect — necking in the deformed solid body followed by its failure.

Thus, during deformation of metallic materials, we come across emerging and developing microscopic instabilities that ultimately result in a macroscopic effect — material failure. This actually means that a solid body shall have some properties that are self-similar at various large-scale or structural levels. Mandelbrot introduced a fractal concept in 1975 to describe such properties [15]. Unlike averaged characteristic, fractal analysis is a versatile tool that makes it possible to analyze the plastic deformation process at various structural levels from a unified perspective and

associate the macroscopic properties of a material to microscopic properties of a defect structure. Identity of kinetic equations and their nonlinearities at various scale levels of the system is the main reason for occurrence of fractal systems in the deformed solid body.

At this point, there is a number of publications containing the findings of both theoretic analysis and quantitative estimation of the fractal dimension of defect structure in plastic yield [16–22]. Structures inside a material (cellular dislocation configurations, for example [17]), and structures on the surface of a material (slip bands, for example [19]) may serve as such. It should be noted that modern experimental techniques associated, in particular, with the investigation of surface texture directly during plastic deformation make it possible to investigate not only metallic materials, but also thin foils [23,24] that, due to their dimensional anisotropy, can exhibit unique properties, including self-similar ones.

Thus, structures on the surface of the deformed body as well as dislocation structures and configurations inside the deformed material are self-similar. During plastic deformation of a metal sample, a strain texture is formed on its surface as a result of strain micromechanisms taking place during plastic yielding of the sample. A recent comprehensive review [25] covers some experimental and computational analyses of strain texture formation and development patterns on free surface of metals and alloys during their plastic deformation.

It is intuitive that quantitative properties of texture are defined by a substructure and microstructure that evolve during plastic deformation, i.e. fractal dimension of the

deformed solid body surface is unambiguously interrelated with fractal dimension of dislocation configurations inside a solid body.

In this sense, a properly built technique for testing a deformed solid body surface to extract fractal dimension of the surface using modern methods of applied mathematics is important because behavior of this property in strain hardening can adequately reflect microstructure evolution inside the material and, thus, indicate structural changes until degradation and subsequent failure of metals and alloys.

Description of the material defect structure during strain impacts and establishment of one-to-one correspondence between fractal properties of this structure and experimentally determined mechanical properties would make it possible to forecast perspective materials during various strain impacts using the obtained knowledge on the features of defect assembly evolution and macroscopic conditions of the experiment. Therefore, in terms of experimental implementation of this approach, this study is devoted to the development of a surface testing technique for a solid body deformed directly in the test zone using modern precision tooling. In addition, fractal dimension extraction by various modern applied mathematics methods will be shown and possible correlations between the experimental data obtained herein and by other researchers will be provided.

2. Experimental and computational techniques

A polycrystalline copper sample with a purity of 99.9% for mechanical test has been prepared as specified in ASTM E08-91. The sample gauge length was 10 mm and cross-section was 4×2 mm. The sample was machined and polished to mirror finish. The prepared sample was annealed in vacuum at 1000 K, annealing time was 2 h. After annealing, the average grain size in the polycrystalline copper sample was about 100...200 mkm.

For uniaxial deformation of the sample, Kammrath–Weiss compact (dimensions $25 \times 16 \times 2$ cm) static test machine (Germany) was used to perform compression/tension with force from 0 to 10 kN. It is featured by the opposite cross-bar movement mechanism that avoids displacement of the sample gauge length to the field of view of the microscope or video camera during testing. And while previously the test had been stopped at various strain levels in other surface measurement studies, the sample was removed from the machine grips and placed on the microscope beam table, the proposed uniaxial deformation experiment stopped the motion drive with preservation of the force loading on the sample and the surface texture, formed by that time of deformation, was read in stressed condition. The test machine itself and the sample were in the field of view of Zygo NewView 7100 optical profilometer that was used for noncontact 3D measurement of the surface topography by the scanning white light interferometry. This profilometer

has a resolution along the x and y axes of about 300 nm and a vertical resolution along the z axis of at least 1 nm. The test area in the x – y plane was 3700×3700 pixels (1084×1084 mkm, 1 pixel = 293 nm). Figure 1 shows the general view of Zygo NewView 7100 optical profilometer (Figure 1, *a*), Kammrath–Weiss static test machine in the field of view of the optical profilometer (Figure 1, *b*), deformed sample surface (Figure 1, *c*) and typical vertical surface profile (empirical 2D model) measured using this optical profilometer (Figure 1, *d*). It should be noted that the image of the typical deformed sample surface profile (Figure 1, *d*) clearly visualizes the strain texture in the form of slip bands that have occurred as a result of dislocation assembly evolution.

During uniaxial deformation at a uniform grip velocity of 300 mkm/min, sample tension was stopped at engineering stresses of 0; 20; 40; 80; 160; 195 and 200 MPa, and the surface texture formed by that time of deformation was read.

The surface texture readings represented a 3700×3700 square matrix filled with height values of the z axis in mkm. The preliminary data review and processing included interpolation of gaps, linear trend removal and outlier filtering that was performed by the Gaussian process regression method [26]. The essence of the method was in approximation of the observed heights by the Gaussian process using the Bayesian regression [26]. Then, the real heights and approximated heights were compared at each point on the coordinate grid. At points where the absolute difference between the real and approximated heights exceeded the pre-defined threshold, the real values were replaced with the simulated ones. It should be noted that the surface profiles measured at the beginning of loading (at lower mechanical stresses) have more artefacts in the form of sharp outliers that are successfully removed by filtering. At the same time, the surface profiles obtained at higher mechanical stresses are almost free of these artefacts.

Figure 2 shows an example of a linear surface transect profile before and after filtering.

The preliminary data review and processing provided the vertical profiles of the test surface at various engineering mechanical stresses. Application of the techniques described above is illustrated in Figure 3 by colored vertical profiles of the test surface at engineering mechanical stresses of 80; 160; 195 and 200 MPa. Figure 3 shows a surface fragment of 1084×1084 mkm. Colored vertical profiles of the test surface at engineering stresses of 0; 20 and 40 MPa are almost uniform in color range (yellow) which generally reflects the absence of plastic yielding related to elastic deformation below the yield strength that is equal to 55 MPa for this sample.

Figure 3 illustrates the sequence of vertical surface profile variation during plastic yielding and confirms that the sample gauge length is not displaced into the field of view of the optical profilometer during testing.

Modern computational methods are used to obtain the necessary properties of surfaces (including fractal ones)

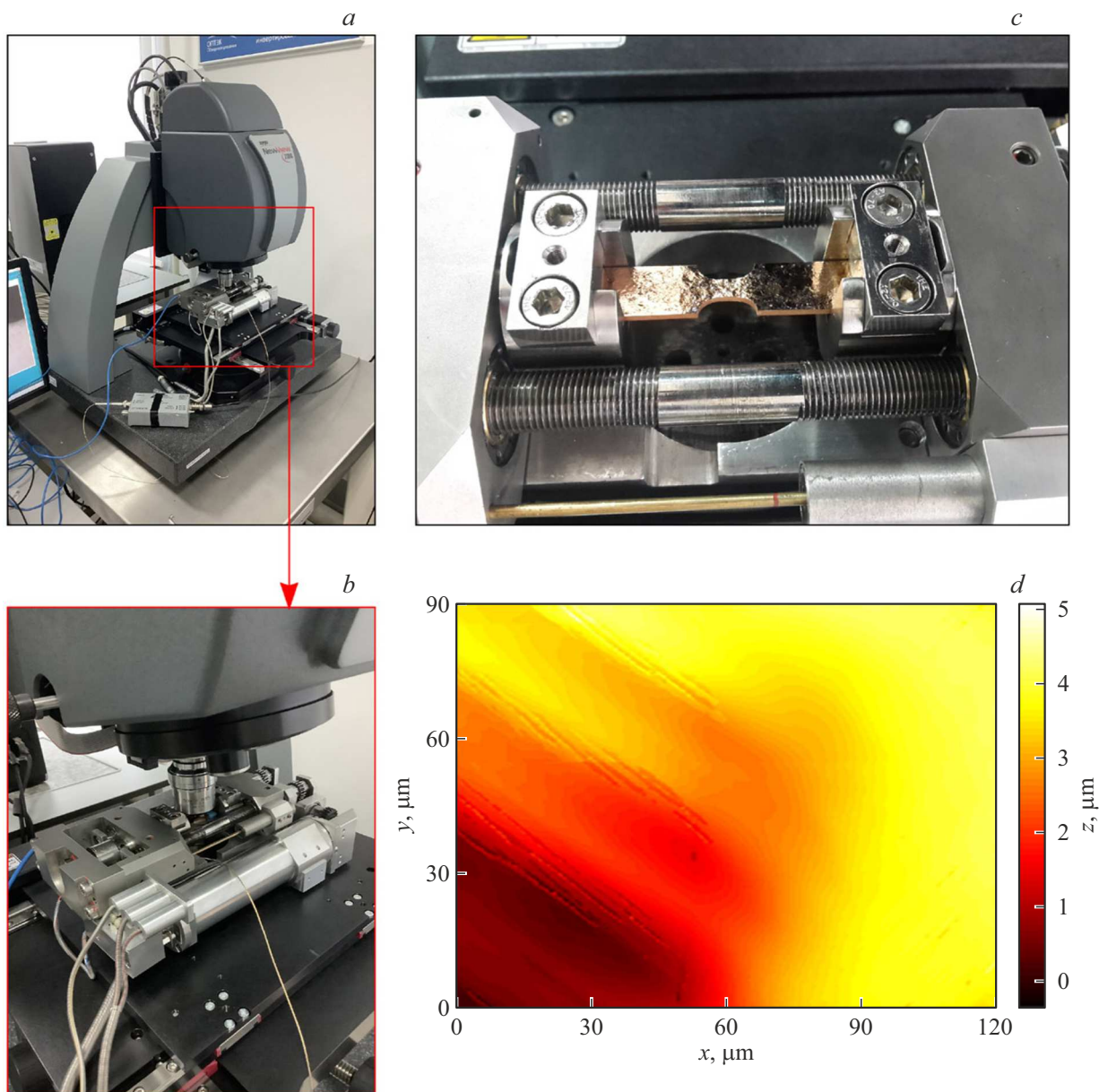


Figure 1. General view of Zygo NewView 7100 optical profilometer (*a*), Kammrath–Weiss static test machine in the field of view of the optical profilometer (*b*), deformed sample surface (*c*) and typical vertical surface profile (empirical 2D model) measured using this optical profilometer (*d*).

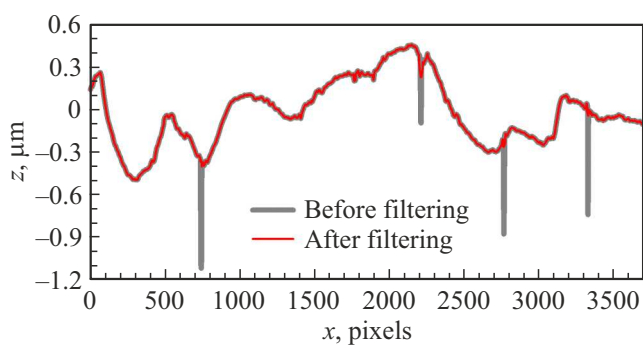


Figure 2. Linear surface transect profile before (gray curve) and after (red curve) filtering.

through the analysis of numerical series and Two-/three-dimensional sets (profiles). Despite its popularity, the *box counting method* — the best known fractal dimension estimation method is currently inferior to new methods both in the computation speed and accuracy. In particular, [27] shows exhaustive comparison of fractal dimension estimation methods in terms of the modern statistical analysis. By assuming that a Gaussian random field (the Gaussian process generalization to two or more dimensions) is a suitable model for the test surface profiles, several methods that used exactly the Gaussian field properties were developed to estimate the fractal dimension of surfaces. It should

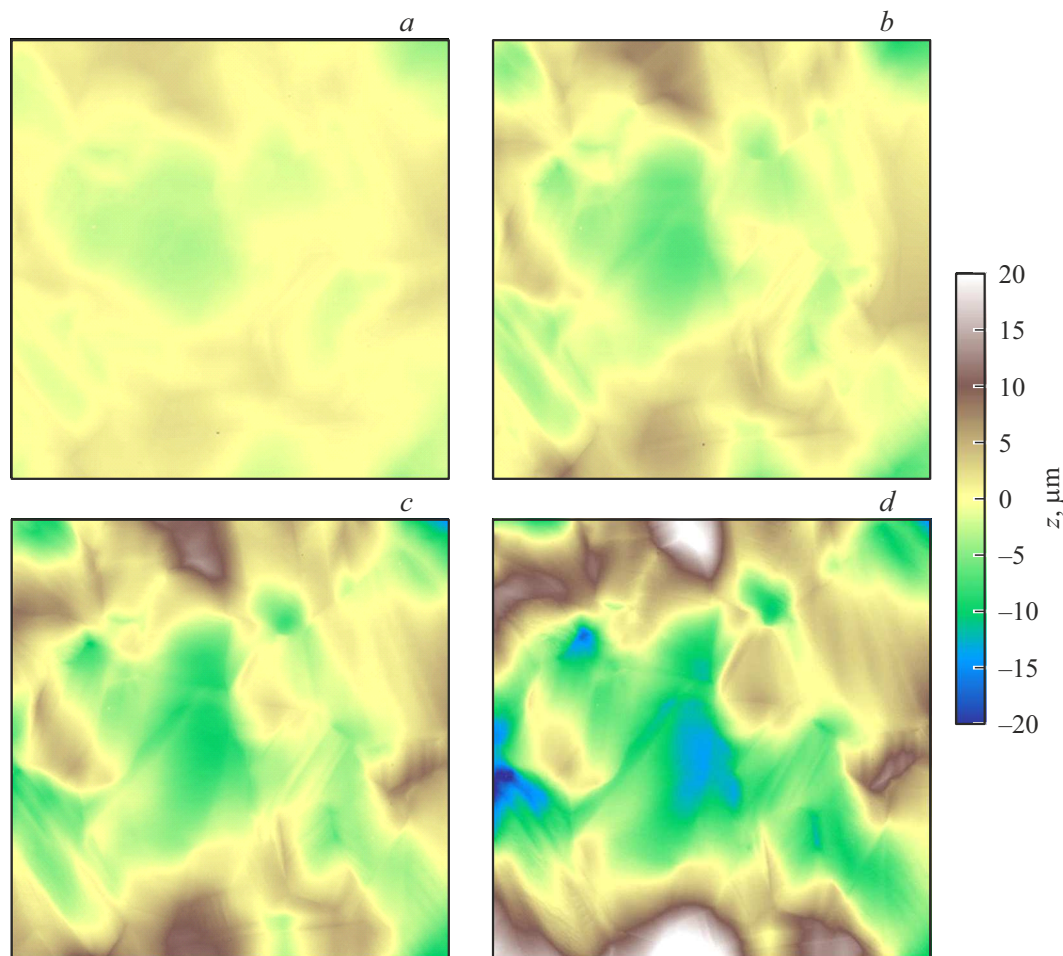


Figure 3. Colored vertical profiles of the test surface at engineering mechanical stresses of 80 (a); 160 (b); 195 (c) and 200 (d) MPa. Surface size is 3700×3700 pixels (1084×1084 mkm, 1 pixel = 293 nm).

be noted that these methods are used most frequently to analyze all kinds of topographic data in geophysics [28], but are often encountered in various areas of physics [29], ecology [30] and other sciences.

This study used three fractal dimension evaluation methods. The first two methods, transect variation estimation and transect increment estimation, were limited to the one-dimensional Gaussian field analysis. Fractal dimension in this case was calculated for all transects (profiles) by two-dimensional height matrix rows and columns. Median of the calculated fractal dimension distribution increased by one gave the estimated fractal dimension of the surface itself. The transect variation estimation for simultaneous calculation of required parameters used two Gaussian random field points, while the transect increment estimation method used three points (difference scheme equivalent in the Gunge–Kutta method). The third method — square increment estimation was limited to the two-dimensional Gaussian field and used four random field points. The necessary mathematical procedures for these methods are adequately addressed in [31] and briefly described in the appendix hereto.

All three methods were implemented using the sliding window scheme: fractal dimension was calculated by averaging several values obtained in the window 2000×2000 pixels in size (1 pixel = 293 nm) sliding at intervals of 500 pixels throughout the surface. With initial surface condition (0 MPa) and achieved maximum stress (200 MPa) for the statistical data set, several fragments with different surface texture of the deformed portion of the sample were read. In this case, averaging was performed on all surface fragments for this stress value.

3. Experimental findings and discussion

As mentioned above, during uniaxial deformation at a uniform grip velocity, sample tension was stopped at engineering mechanical stresses of 20; 40; 80; 160; 195 and 200 MPa, and the surface texture formed by that time of deformation was read. After mathematical processing of the textures, fractal dimension of the sample surface was estimated at the specified values of the achieved engineering mechanical stress by three methods: transect

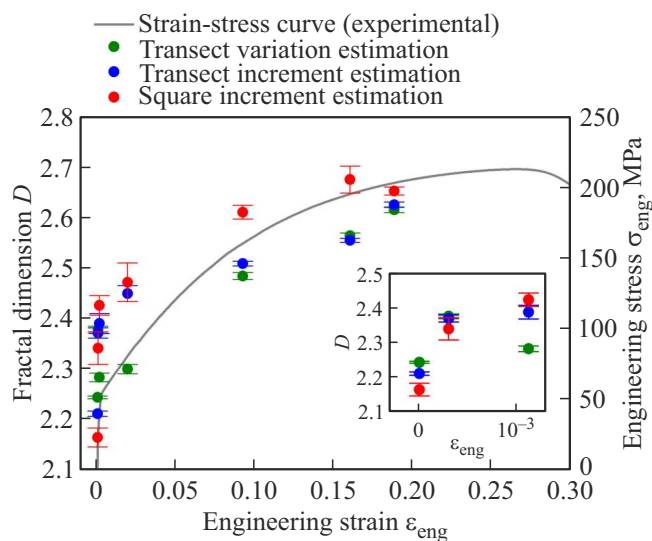


Figure 4. Loading curve of the polycrystalline copper sample in the engineering coordinates „relative strain–mechanical stress“ and fractal dimensions calculated by the three methods addressed herein.

variation estimation, transect increment estimation and square increment estimation.

Figure 4 shows the loading curve of the polycrystalline copper sample in the engineering coordinates „relative strain — mechanical stress“, and fractal dimensions calculated by the three methods at the relative strains corresponding to the chosen mechanical stresses.

Initial condition of unstressed sample surface (0 MPa) shall correspond to a mirror flat surface and its fractal dimension shall be equal to the Euclidean dimension, i.e. 2, but the values calculated by the three methods are within 2.15...2.25. Displacement of the fractal dimension from the Euclidean dimension by 0.15...0.25 might be caused by a group of factors: surface cleanliness (the sample surface is a non-ideal flat optical reflector in the initial condition) and by optical and computational noise of hardware and processing algorithms.

At the initial loading of the sample up to the yield strength (engineering stresses of 20 and 40 MPa), the fractal dimension grows to 2.3...2.4, which is shown in the Detail in Figure 4. We believe that fractal properties of the surface vary due to the defect (dislocation) assembly evolution that, basically, shall be absent below the yield strength. However, the observed increase in the fractal dimension may be caused by activation of easy glide in separate crystallites (grains) located on the surface and favorably oriented to activation of the easy dislocation glide systems at low engineering stresses. Thus, the surface texture to be formed may be described as occurrence of rare, but long slip lines with a low height (several Burgers vector units) in separate grains, which is shown in Figure 1, *d*. At the initial sample loading stage (Detail in Figure 4), there is some discrepancy in the fractal dimensions estimated

by the chosen methods. When the engineering strain is about 10^{-3} (engineering stress is 40 MPa), the transect variation estimation shows the fractal dimension lower than the values calculated by other two methods. We suppose that this may be associated with the number of generalized difference variation arguments for the random field values (see the Appendix). The first method (transect variation estimation) uses two random field values in iteration, the second method (transect increment estimation) uses three values and the third method (square increment estimation) uses four values. Increase in the random field values for iteration increases the probability that a slip line fragment will get into the calculation iteration and, therefore, that the obtained fractal dimension will increase.

With further increase in the engineering stress (80; 160; 195 MPa), classical stress-strain behavior is observed and corresponds to strain hardening followed by the increasing fractal dimension trend up to 2.65 (Figure 4). Again, it should be noted that there is some discrepancy in absolute estimated fractal dimension values by the three methods at engineering stresses of 80; 160 and 195 MPa, but the general smooth growth trend of the fractal dimensions is not disturbed. The difference in absolute values is probably caused by the same ratio of the number of generalized difference variation arguments for the random field values and by the strain texture features. With increase in sample stress and total strain, groups of slip lines, elastic-plastic strain zones at grain boundaries (Figure 3, *a*), signs of cross slip (Figure 3, *b*) and considerable increase in the surface height range (Figure 3, *c*) may be observed on the surface and demonstrate that high plastic deformation has been accumulated and some grain shapes have been distorted.

The final loading stage was the achieved engineering stress of 200 MPa that appeared to be quite close to the ultimate strength of 215 MPa. However, strain localization with necking was not observed at such stress and the material retained the acceptable stress-induced plastic yield stability for qualitative recording of the strain texture. Figure 3, *d* shows the achieved properties of the strain texture as a result of plastic yield of the material such as drastic change in some grain boundaries, grain surface filling with a dense grid of slip lines, significant height differences that form the texture. It should be noted that all three methods show very close fractal dimensions at this experiment point.

Since the measurements, calculations or simulation of fractal dimension on the polycrystalline copper surface have been performed before by other authors, then it is not unreasonable to compare the values achieved herein with the values of other authors within this guidance paper. Fractal dimensions vs. relative shear stress measured in $10^{-3}G$ (G — shear modulus) will be shown. Actually, according to the Taylor relation ($\tau = \alpha G b \sqrt{\rho}$, where τ is the true shear stress, $\alpha \sim 0.5$ is the geometrical factor that is weakly dependent on the temperature, b is the Burgers vector, ρ is the density of dislocations), such choice of an argument makes it dependent only on the density of

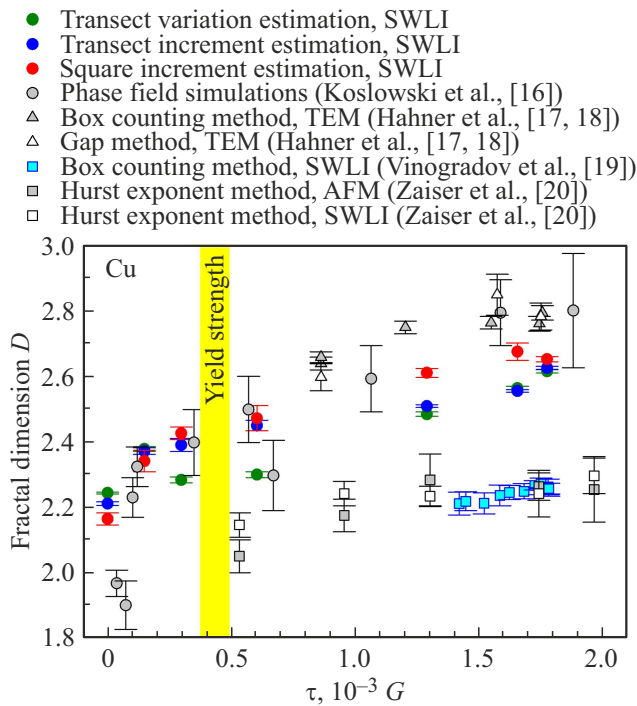


Figure 5. Results of fractal dimension estimation by three methods addressed herein and results obtained by other authors (the legend lists the fractal dimension calculation method, experimental procedure and reference to the corresponding studies). The range of stresses corresponding to the yield strength of the polycrystalline copper are shown in yellow.

dislocations, i.e. its evolution is supposed to govern the fractal property variation of the surface. Therefore, all analyzed experimental data may be unified in terms of dependence only on the governing property — density of dislocations, and, in future, materials with different strain-stress properties may be compared on a single diagram.

Figure 5 shows the results of fractal dimension estimation by the three methods described by us and the results achieved by other authors. They are addressed in detail below.

In [16], a 2D dislocation model of a phase field was used to simulate the dislocation structure in a single slip plane (*phase field simulation*). In this model, the dislocation assembly was represented by an integer scalar phase field whose values at each point prescribed the shear in the Burgers vector units. Scalar field jumps defined the dislocation line arrangement and random obstacles simulated forest dislocations. The scalar field values at each point of time were calculated in the pre-defined initial conditions using the real parameters of the polycrystalline copper assuming the work minimization principle. Frequency distribution of the constant scalar field areas (shear within such areas remained unchanged from point to point) was approximated by the inverse exponential function whose exponent increased by one provided the estimated fractal dimension.

In [17,18], uniaxial tension tests were carried out along axis [100] of the pure copper single crystals. Images of the cellular dislocation substructure made by the transmission electron microscopy were digitalized and binarized. Fractal dimension was calculated by the *box counting method*. The method was used to plot the dependence of the number of boxes containing at least one dislocation grid point on the box side length. The dependence was approximated by the inverse power law and the exponent plus one gave the estimated fractal dimension. Authors of [17,18] also described another fractal dimension calculation method that was based on the count of dislocation cells whose size exceeded the set out threshold (*gap method*). The cell size measurement procedure was not defined. Dependences of the number cells on the threshold were approximated by the inverse power law and the exponent increased by one gave the estimated fractal dimension.

In [19], uniaxial tension tests were carried out on pure (99.98%) polycrystalline copper. Surface measurements were made at different deformation values using the scanning white light interferometer and the macroscopic surface curvature effects were neutralized. Fractal dimension was calculated by the *box counting method* that was used to plot a dependence of the number of cubes containing at least one surface point on the cube side length. The dependence was approximated by the inverse power law and the exponent gave the estimated fractal dimension. The resulting fractal dimension at each deformation value was calculated by averaging several measurements made in different areas in the center of the sample.

In [20], uniaxial tension tests were carried out on pure (99.99%) polycrystalline copper. Surface measurements at various deformation levels were carried out using the atomic-force microscope and white light interferometer. Two to five linear profiles on the tension axis were taken from each surface and two to three profiles in the perpendicular direction were taken. Each profile was used to calculate the height difference with the height spacing that was assumed as the argument. The dependence was approximated by the power law with an exponent unambiguously related to the fractal dimension by a linear transformation (*Hurst exponent method*). Fractal dimension for each deformation value was calculated by averaging of several profiles separately for the atomic-force microscope and white light interferometer.

All shown results with possible errors exhibit a rising trend within the test unified shear stress range. Moreover, two groups of results may be distinguished. The first group ([19,20]) exhibit the fractal dimension growth in the range of about 2.0...2.2 and the second group ([16–18] and herein) exhibit the fractal dimension growth above the yield strength in the range of about 2.3...2.8.

At this point, it is still a debated question whether such „offset“ of one group of results relative the other group is caused by the features of the computational methods or by sample preparation that changes the fractal dimension of the initially unloaded sample upwards from the Euclidean

dimension. However, the fact that the fractal dimension and stress (and, thus, the density of dislocation assembly) are in one-to-one correspondence suggests that the fractal dimension unambiguously if not fully reflects the dislocation assembly evolution during the plastic yield process.

It should be noted that the equivalent fractal dimension behavior was observed on the amorphous glass surfaces [32]. This is probably due to the shear band vertices that represent dislocation-type defects [33] which means that their behavior may perfectly correlate with the dislocation assembly behavior in metallic materials. This fact is rather controversial, however, it is interesting in terms of common flow of deformation processes in different condensed media and detection of common properties (in particular, fractal dimension of the defect assembly) to allow unambiguous description of such processes.

4. Conclusion

The study demonstrates an experimental surface test technique for the polycrystalline copper in uniaxial deformation that was performed using the compact test machine with the opposite cross-bar movement mechanism directly in the field of recording of the white light interferometer. The data obtained experimentally on the same surface area were analyzed by modern computational methods and fractal dimensions were calculated at different applied stresses. The fractal dimension demonstrated the rising trend in the stable plastic yield area from the yield strength almost to its instability point. Comparison of the results obtained herein with the results of other authors did not show any obvious discrepancies in the fractal dimension behavior that was discussed herein, but rather identified the features and patterns of the utilized computational methods. Though the modern computational methods used by the research community do not change the general picture of the rising fractal dimension trend during plastic yielding of the test sample, they can result in the „datum“ drift or demonstrate sensitivity to certain plastic yield stages. Nevertheless, the obtained one-to-one correspondences between the fractal dimension and stress that is associated with the density of dislocations through the Taylor relation demonstrate the role of the fractal dimension as an unambiguous indicator of the dislocation assembly state in plastic yielding.

Funding

The study was supported financially by the Russian Science Foundation as part of research project No. 24-29-00087.

Conflict of interest

The authors declare that they have no conflict of interest.

Appendix (Supplementary materials)

As mentioned above, this study used three fractal dimension evaluation methods. All these methods are based on the analysis of the Gaussian fields with different sizes. Let's introduce some mathematical notations. Given a d -dimensional random field X_t written as

$$\{X_t : t \in R^d\}. \quad (1)$$

Here, t are coordinates in the d -dimensional space. In practice, the coordinates are only set in the regular grid vertices. In our case, coordinates of the square grid where the 2D field values are set are defined as normalized to the number of points on the square grid side

$$t = \begin{pmatrix} t_1 \\ t_2 \end{pmatrix} = \frac{1}{n} \begin{pmatrix} i_1 \\ i_2 \end{pmatrix}, \text{ where } i_1, i_2 = 1, 2, \dots, n, \quad (2)$$

where i_1, i_2 are grid indices, n is the number of points on the square grid side.

Further, a variogram notion is introduced. This means a random field value difference variation in two point as function of the point spacing. For this purpose, the variogram describes the degree of data difference depending on the data spacing. The generalized variogram of degree p ($p > 0$) is written as

$$\gamma_p(t) = \frac{1}{2} E[|X_u - X_{u+t}|^p], \quad (3)$$

where E is the expected value and the difference of random field values in two points is taken by the absolute value. Assuming that X_t in the Gaussian random field, the variogram at $t \rightarrow 0$ satisfies the expression

$$\gamma_p(t) \sim \|ct\|^{\frac{\alpha}{2}p}, \quad (4)$$

where $\alpha \in (0, 2]$, c is some constant and double square brackets denote the Euclidean norm. The fractal dimension is related to α by the following expression:

$$D = d + 1 - \frac{\alpha}{2} \quad (5)$$

and, accordingly, the fractal dimension estimation is limited to calculation of α .

Two fractal dimension estimation methods of the surface that are limited to a one-dimensional case: the *transect variation estimation* and *transect increment estimation*, use the two-dimensional height matrix rows and columns. The fractal dimension is calculated in this case for all transects (profiles) that are defined as a one-dimensional random field $\{X_t : t = \frac{i}{n}\}$, where $i = 1, 2, \dots, n$. Median of the calculated fractal dimension distribution plus one gives the estimated fractal dimension of the surface itself.

The transect estimation of the fractal dimension is defined by the expression:

$$\hat{D}_{V,p} = 2 - \frac{1}{p} \left\{ \sum_{l=1}^L (s_l - \langle s \rangle) \log V \left(\frac{l}{n} \right) \right\} \times \left\{ \sum_{l=1}^L (s_l - \langle s \rangle)^2 \right\}^{-1}. \quad (6)$$

Here, $L \geq 2$ (for calculations, $L = 2$ is generally chosen), $s_l = \log \frac{l}{n}$ and $\langle s \rangle = \frac{1}{L} \sum_{l=1}^L s_l$. The actual fractal dimension is defined as the slope of linear dependence of $\log V \left(\frac{l}{n} \right)$ on $\log \frac{l}{n}$.

The *transect variation estimation* uses the generalized first-order difference variation as $V(l/n)$:

$$\hat{V}_p^{(1)} \left(\frac{l}{n} \right) = \frac{1}{2(n-l)} \sum_{i=1}^n |X_{i/n} - X_{(i-l)/n}|^p. \quad (7)$$

The *transect increment estimation* uses the generalized second-order difference variation as $V(l/n)$:

$$\hat{V}_p^{(2)} \left(\frac{l}{n} \right) = \frac{1}{2(n-2l)} \sum_{i=1}^{n-l} |X_{(i+l)/n} - 2X_{i/n} + X_{(i-l)/n}|^p. \quad (8)$$

The third fractal dimension estimation method is related to a 2D random field. This is the *square increment estimation* that is based on the generalized square increment variation $\hat{V}_{SI,p} \left(\frac{k}{n} \right)$ written as

$$\hat{V}_{SI,p} \left(\frac{k}{n} \right) = \frac{1}{2N(k)} \sum_{S(k)} |X_{i_1/n, i_2/n} - X_{i_1/n, j_2/n} - X_{j_1/n, i_2/n} + X_{j_1/n, j_2/n}|^p. \quad (9)$$

Here, summation is performed within the following set

$$S(k) = \left\{ (i_1, i_2, j_1, j_2) \in \{0, 1, \dots, n\}^4 : \left\| \begin{pmatrix} i_1 \\ i_2 \end{pmatrix} - \begin{pmatrix} j_1 \\ j_2 \end{pmatrix} \right\| = k \right\}, \quad (10)$$

where k is the distance and $N(k)$ is the cardinal number of $S(k)$.

The square increment estimation of fractal dimension is written in a similar way as (6):

$$\hat{D} = 2 - \frac{1}{p} \left\{ \sum_{k \in K} (s_k - \langle s \rangle) \log \hat{V}_{SI,p} \left(\frac{k}{n} \right) \right\} \times \left\{ \sum_{k \in K} (s_k - \langle s \rangle)^2 \right\}^{-1}. \quad (11)$$

Here, $s_k = \log \frac{k}{n}$. The actual fractal dimension is defined as the slope of linear dependence of $\log \hat{V}_{SI,p} \left(\frac{k}{n} \right)$ on $\log \frac{k}{n}$, where $K = \{\sqrt{2}, 2\sqrt{2}\}$.

References

- [1] Michael F. Ashby, David R.H. Jones. Engineering Materials. An Introduction to Properties, Applications and Design. Elsevier, Holland (2006). V. 1, 439 p. V. 2. 466 p.
- [2] Günter Gottstein. Physical Foundations of Materials Science. Springer-Verlag, Berlin (2004). 510 p.
- [3] D. Kondepudi, I. Prigogine. Modern Thermodynamics. From Heat Engines to Dissipative Structures. John Wiley & Sons (2014). 560 p.
- [4] H. Mecking, U.F. Kocks. Acta Metallurgica **29**, *11*, 1865 (1981).
- [5] Y. Estrin, H. Mecking. Acta Metallurgica **32**, *1*, 57 (1984).
- [6] G.A. Malygin. Phys.–Usp. **42**, *9*, 887 (1999).
- [7] L.P. Kubin, C. Fressengeas, G. Ananthakrishna. Dislocation in Solids. Ch. 57. Collective Behaviour of Dislocations in Plasticity. Elsevier Science (2002). P. 101–192.
- [8] U.F. Kocks, H. Mecking. Prog. Mater. Sci. **48**, *3*, 171 (2003).
- [9] I.S. Yasnikov, A. Vinogradov, Yu. Estrin. Phys. Solid State **55**, *2*, 346 (2013).
- [10] M.C. Carmen-Miguel, A. Vespignani, S. Zapperi, J. Weiss, J.R. Grasso. Nature **410**, 667 (2001).
- [11] T. Richeton, J. Weiss, F. Louchet. Nature Mater. **4**, 465 (2005).
- [12] D.M. Dimiduk, C. Woodward, R. LeSar, M.D. Uchic. Science **312**, 5777, 1188 (2006).
- [13] I.S. Yasnikov, A. Vinogradov, Y. Estrin. Scripta Mater. **76**, 37 (2014).
- [14] E.A. Agletdinov, I.S. Yasnikov. Phys. Rev. E **108**, *4*, 044217 (2023).
- [15] B.B. Mandelbrot. The Fractal Geometry of Nature. Henry Holt and Company. (1983). 468 p.
- [16] M. Koslowski, R. LeSar, R. Thomson. Phys. Rev. Lett. **93**, *26*, 265503 (2004).
- [17] P. Hähner, K. Bay, M. Zaiser. Phys. Rev. Lett. **81**, *12*, 2470 (1998).
- [18] M. Zaiser, K. Bay, P. Hähner. Acta Mater. **47**, *8*, 2463 (1999).
- [19] A. Vinogradov, I.S. Yasnikov, Y. Estrin. Phys. Rev. Lett. **108**, *20*, 205504 (2012).
- [20] M. Zaiser, F.M. Grasset, V. Koutsos, E.C. Aifantis. Phys. Rev. Lett. **93**, *19*, 195507 (2004).
- [21] I. Groma, B. Bakó. Phys. Rev. Lett. **84**, *7*, 1487 (2000).
- [22] S. Lipseői, S. Kalácska, P.D. Ispánovity, J.L. Lábár, Z. Dankházi, I. Groma. Phys. Rev. Mater. **7**, *3*, 033604 (2023).
- [23] V.E. Korsukov, A.V. Ankudinov, V.I. Betekhtin, P.N. Butenko, V.N. Verbitskii, V.L. Hilarov, I.V. Hilarov, S.A. Knyazev, M.M. Korsukova, B.A. Obidov. Phys. Solid State **62**, *12*, 2249 (2020).
- [24] B.A. Obidov, V.E. Korsukov, V.L. Hilarov, A.V. Ankudinov, P.N. Butenko, S.A. Knyazev, M.M. Korsukova. Phys. Solid State **64**, *8*, 925 (2022).
- [25] E.S. Emelianova, O.S. Zinovieva, V.A. Romanova, R.R. Balakhonov, M. Pisarev. Phys. Mesomech. **27**, *1*, 16 (2024).
- [26] C.E. Rasmussen, C.K.I. Williams. Gaussian Processes for Machine Learning. The MIT Press, Massachusetts, USA (2006). 266 p.
- [27] T. Gneiting, H. Ševčíková, D.B. Persival. Statistic. Sci. **27**, *2*, 247 (2012).
- [28] J.A. Goff, T.H. Jordan. J. Geophys. Res. Solid Earth **93**, *B11*, 13589 (1988).
- [29] M. Cavagliá. Classical Quantum Gravity **39**, *13*, 135012 (2022).

- [30] L.H.L. Loke, R.A. Chisholm. *Ecology Lett.* **25**, 10, 2269 (2022).
- [31] R.J. Adler. *The Geometry of Random Fields*. Wiley, N.Y. (1981). 280 p.
- [32] V.E. Korsukov, A.V. Ankudinov, V.I. Betekhtin, P.N. Butenko, V.N. Verbitskii, V.L. Gilyarov, M.M. Korsukova, M.V. Narykova, B.A. Obidov. *Phys. Solid State* **61**, 4, 585 (2019).
- [33] A. Vinogradov, M. Seleznev, I.S. Yasnikov. *Scripta Mater.* **130**, 138 (2017).

Translated by E.Iinskaya